Alzheimer's & Dementia 14 (2018) 1022-1037

Featured Article

Doublecortin expression in CD8+ T-cells and microglia at sites of amyloid-β plaques: A potential role in shaping plaque pathology?

Michael S. Unger[a,b], Julia Marschallinger[a,b,c], Julia Kaindl[a,b], Barbara Klein[a,b], Mary Johnson[d], Ahmad A. Khundakar[d], Steffen Roßner[e], Michael T. Heneka[f], Sebastien Couillard-Despres[b,g], Edward Rockenstein[h], Eliezer Masliah[h], Johannes Attems[d], Ludwig Aigner[a,b,*]

[a]Institute of Molecular Regenerative Medicine, Paracelsus Medical University, Salzburg, Austria
[b]Spinal Cord Injury and Tissue Regeneration Center Salzburg (SCI-TReCS), Paracelsus Medical University, Salzburg, Austria
[c]Department of Neurology and Neurological Sciences, Stanford University School of Medicine, Stanford, CA, USA
[d]Institute of Neuroscience, Newcastle University, Newcastle upon Tyne, UK
[e]Paul Flechsig Institute for Brain Research, University of Leipzig, Leipzig, Germany
[f]University Hospital Bonn, Clinic and Polyclinic for Neurology, Clinical Neuroscience, Bonn, Germany
[g]Institute of Experimental Neuroregeneration, Paracelsus Medical University, Salzburg, Austria
[h]Department of Neuroscience, School of Medicine, University of California San Diego, San Diego, CA, USA

Abstract

Introduction: One characteristic of Alzheimer's disease is the formation of amyloid-β plaques, which are typically linked to neuroinflammation and surrounded by inflammatory cells such as microglia and infiltrating immune cells.

Methods: Here, we describe nonneurogenic doublecortin (DCX) positive cells, DCX being generally used as a marker for young immature neurons, at sites of amyloid-β plaques in various transgenic amyloid mouse models and in human brains with plaque pathology.

Results: The plaque-associated DCX+ cells were not of neurogenic identity, instead most of them showed coexpression with markers for microglia (ionized calcium-binding adapter molecule 1) and for phagocytosis (CD68 and TREM2). Another subpopulation of plaque-associated DCX+ cells was negative for ionized calcium-binding adapter molecule 1 but was highly positive for the pan-leukocyte marker CD45. These hematopoietic cells were identified as CD3-and CD8-positive and CD4-negative T-cells.

Discussion: Peculiarly, the DCX+/ionized calcium-binding adapter molecule 1+ microglia and DCX+/CD8+ T-cells were closely attached, suggesting that these two cell types are tightly interacting and that this interaction might shape plaque pathology.

Keywords: Doublecortin (DCX); Microglia; T-cells; Alzheimer's disease

1. Introduction

Alzheimer's disease (AD) is characterized by a progressive loss of cognitive functions [1,2]. Formation of neurofibrillary tangles (NFTs) and amyloid-β plaques is described as major neuropathological hallmarks of AD, and several transgenic mouse models are designed to produce amyloid-β plaques and/or tau pathologies and to mimic the cognitive deficits of AD for studying AD pathogenesis [3,4]. Neuroinflammation, especially the activation of microglia is heavily debated to contribute to disease progression and to worsen late-stage pathology [5–7]. Microglia cells are located directly at sites of amyloid deposits in AD brains, where they are supposed to phagocytose the amyloid plaque material [8,9]. Several reports suggest that in more advanced stages of plaque pathology and AD, microglia become increasingly dysfunctional in phagocytosis, in cell proliferation,

Conflict of interest: The authors declare that there is no conflict of interest.

*Corresponding author. Tel.: +43 (0)662 2420 80 800; Fax: +43 (0)662 2420 80809.
E-mail address: ludwig.aigner@pmu.ac.at

https://doi.org/10.1016/j.jalz.2018.02.017

motility, signaling, and in proteostasis, all contributing to an altered microglia phenotype [10]. The occurrence of peripheral immune cells in the brain, specifically T-cells, and their functional role and interaction with brain resident glial cells is currently discussed. For example, there is evidence for increased T-cell homing into the aged but otherwise healthy brain [11, 12]. Moreover, higher T-cell numbers are found in the brains of several amyloid plaque mouse models [13]. However, the specific T-cell subtypes, their functional relevance, and a possible modulatory activity of T-cells in brains with plaque pathology are still controversial [14].

Besides neuroinflammation, altered levels of adult neurogenesis are reported to manifest along AD pathology in several amyloid-β transgenic mouse models [15]. Adult hippocampal neurogenesis is the production of new functional neurons from neural stem and progenitor cells and takes place in specific neurogenic niches in the mammalian brain, namely the subgranular zone of the dentate gyrus and the subventricular zone of the lateral ventricle walls [16–19]. There, stem cells give rise to neuronal progenitor cells, which mature and integrate functionally in the existing neuronal network [20]. The population of neuronal precursors or young immature neurons can be identified by its expression of the microtubule-associated protein doublecortin (DCX) [21,22].

We recently demonstrated changes in hippocampal neurogenesis already at very early stages of disease pathology in transgenic amyloid-β animal models, before the manifestation of amyloid-β plaques [23]. In the frame of this analysis, we made the surprising finding of DCX-immunoreactive cells outside the neurogenic niche at sites of amyloid deposits. Here, we present a detailed analysis of the identity of DCX-immunoreactive cell populations associated with amyloid plaques in cortical and hippocampal brain regions of various transgenic amyloid mouse models and in human brains with plaque pathology and in AD specimen. We report for the very first time on DCX-immunoreactive microglia in amyloid mouse models and on DCX-positive T-cells that presumably infiltrate the brain parenchyma of AD transgenic mice and tightly associated with the resident microglia.

2. Material and methods

2.1. Animals

Female amyloid-β precursor protein (APP) Swedish PS1 dE9 (APP-PS1) mice [24] expressing a chimeric mouse or human mutant amyloid precursor protein (Mo/HuAPP695swe) and a mutant human presenilin 1 (PS1 dE9) both directed to central nervous system neurons under the prion protein promoter (Jackson Laboratory, http://www.jax.org/strain/005864) were used. For brain histology, we analyzed mice at 3, 10, and 13 months of age. Age-matched nontransgenics derived from the breeding of APP Swedish PS1 dE9 were used as control animals. Mice were housed at the University Hospital Bonn–Clinical Neuroscience in groups under standard conditions at a temperature of 22°C and a 12 h light or dark cycle with ad libitum access to standard food and water. Animal care and handling were performed according to the Declaration of Helsinki and approved by local ethical committees. Brain sections of the APP-Lon/Swe mice overexpressing hAβPP751 with the London (V717I) and Swedish (K670M/N671L) mutations [25,26] and the transgenic APP-SDI mouse model overexpressing human amyloid-β precursor protein (APP 770 isoform) with the Swedish K670N/M671L, Dutch E693Q, and Iowa D694N mutations [27,28] were kindly provided by Prof. Christian Humpel (Laboratory of Psychiatry and Experimental Alzheimer's Research, Department of Psychiatry Psychotherapy and Psychosomatic, Medical University of Innsbruck, Austria). Brain sections from transgenic Tg2576 mice [29,30] overexpressing the human APP Swedish mutation and wild type littermates at postnatal ages from 3 to 18 months were kindly provided by Prof. Steffen Roßner (Paul Flechsig Institute for Brain Research, University of Leipzig, Germany). Brain sections from DCX knockout mice (DCX-KO) and age-matched controls [31] were kindly provided by Fiona Francis (Institut du Fer à Moulin, Paris, France). Brain sections of 8-month-old human α-synuclein overexpressing mice (D-line), a model of synucleinopathy and of Lewy body dementia [32–34], were included in the study.

2.2. Behavior test

For analysis of spatial learning and memory function, Morris water maze (MWM) test was performed in accordance with the local Animal Health Commission (BMWFW-66.019/0032-WF/V/3 b/2016). This MWM paradigm was performed as previously published [35]. For behavior analysis, 13- to 15-month-old female and male APP-PS1 and age-matched Nestin-CreERT2/R26R-YFP control animals [35,36] were used (n = 4/group). For the MWM test, a 108 cm round basin arena filled with 22° ± 1°C warm water was used. A 10 × 10 cm square platform was placed 1 cm below the water surface in the maze. Big black cue symbols were put on each wall of the basin and the testing room to allow the animals spatial orientation. The experimental setup was not changed throughout the whole learning session and performed under constant light conditions. Water maze trials (maximum 60 s) for learning were performed twice a day for a total of 5 days. On each trial, every mouse was put in the water and given 60 s to swim and locate the submerged platform. If the platform was not detected within 60 s, the animal was guided onto the platform and allowed to remain there for 10 s to learn the spatial position of the platform. Only on the first trial of day 1, the platform was marked with a black flag to visualize the platform location to the mice. On day 6, an additional

memory paradigm was performed by removing the platform, and mice were tracked for 60 s. The swim path, that is, the total distance moved and the swim speed was recorded using EthoVision software (XT 9.0.726, Noldus). In the absence of the platform during the last session, the time the animals spent in the platform quadrant and the visits in the platform quadrant were additionally calculated.

2.3. Human brain samples

We used 7 μm hippocampal sections from formalin-fixed paraffin-embedded brain samples which were obtained from the Newcastle Brain Tissue Resource in accordance with Newcastle University ethics board and ethical approval awarded by the Joint Ethics Committee of Newcastle and North Tyneside Health Authority (reference: 08/H0906/136).

Irrespective of clinical diagnoses, all brains underwent neuropathological examination according to a routine protocol that uses standardized neuropathological scoring or grading systems, including NFT Braak staging [37,38], Consortium to Establish a Registry for Alzheimer's Disease scores [39], Newcastle/McKeith Criteria for Lewy body disease [40], National Institute on Aging—Alzheimer's Association guidelines [41], and Thal phases of amyloid-β deposition [42]. Our study group consisted of 14 AD cases which showed NFT Braak stages 4-6 and fulfilled the criteria for high AD neuropathological change according to the National Institute on Aging–Alzheimer's Association guidelines [41] and besides classical AD pathology (i.e., NFTs, amyloid plaques, and neuritic plaques) did not show any other pathology (e.g., Lewy bodies, TAR DNA-binding protein 43 positive intracellular inclusions) in the hippocampus. As controls, we used seven cases with NFT Braak stages 0 to 3, which showed no or only very limited amounts of amyloid pathology in the hippocampus.

2.4. Perfusion and tissue processing

APP-PS1 animals were anesthetized and transcardially perfused for immunohistochemistry as previously described [43]. Following perfusion, the brains were extracted and postfixed with 4% paraformaldehyde in sodium phosphate buffer (0.1 M; pH = 7.4) over night at 4°C. The brains were cryoprotected and transferred into 30% sucrose in 0.1 M sodium phosphate buffer (PBS) (pH = 7.4). Sagittal sections of 40 μm were cut on dry ice with a sliding microtome.

2.5. Immunohistochemistry

Fluorescence immunohistochemistry of mouse tissue was performed on free-floating sections as previously described [23,43]. Antigen retrieval was performed depending on the used primary antibody by steaming the sections for 15–20 min in citrate buffer (pH = 6.0, Sigma). The following primary antibodies were used:

Rabbit anti-DCX (1:300, Cell Signaling), normal rabbit IgG control (prediluted to the concentration of rabbit anti-DCX c = 156 μg/mL and finally used at 1:300, Cell Signaling), goat anti–ionized calcium-binding adapter molecule 1 (Iba1) (1:500, Abcam), rat anti-CD45 (1:100, Millipore), mouse anti-Aβ (1:1000, Covance), sheep anti-TREM2 (1:300, R&D Systems), rat anti-CD68 (1:250, Serotec), rat anti-CD3 (1:100, Bio-Rad), rat anti-CD8 (1:100, eBioscience), goat anti-PCNA (1:300, Santa Cruz Biotechnology), mouse anti-Nestin (1:300, Abcam), goat anti-Sox2 (1:1000, Santa Cruz Biotechnology), mouse anti-PSA-NCAM (1:2000, Millipore), chicken anti-GFAP (1:2000, Abcam), goat anti-Olig2 (1:300, R&D Systems), mouse anti-NeuN (1:500, Millipore), rat anti-B220 (1:100, eBioscience), rat anti-Ly6G (1:100, eBioscience), rat anti-CD169 (1:50, Bio-Rad), rat anti-CD4 (1:100, eBioscience), and rat anti-Foxp3 (1:100, eBioscience). For α synuclein staining rat anti-α-synuclein (1:50, Enzo) antibody was used and antibody incubation time was increased for a total of 2 days.

Sections were extensively washed in PBS and incubated for 3 h at room temperature (RT) in secondary antibodies all diluted 1:1000. The following secondary antibodies were used: donkey anti-rabbit Alexa Fluor 568 or Alexa Fluor 647, donkey anti-goat Alexa Fluor 568, donkey anti-rat Alexa Fluor 488 or Alexa Fluor 568, donkey anti-sheep 488, donkey anti-mouse Alexa Fluor 568 (all Invitrogen or Molecular Probes), donkey anti-rat Rhodamine Red, donkey anti-mouse AF647, donkey anti-goat AF647, donkey anti-chicken Alexa Fluor 647, donkey anti-rat AF647 (all Jackson ImmunoResearch). Nucleus counterstaining was performed with 4′,6′-diamidino-2-phenylindole dihydrochloride hydrate (DAPI 1 mg/mL, 1:2000, Sigma). For qualitative amyloid-β plaque staining, Thioflavin S (1 mg/mL, 1:625, Sigma) was added to the secondary antibody solution. Mouse tissue sections from AD brains were additionally treated with 0.2% Sudan Black (Sigma) in 70% ethanol for 1–2 minutes to reduce the autofluorescence in tissue from old animals [44]. After this treatment, the sections were extensively washed in PBS and mounted onto microscope glass slides (Superfrost Plus, Thermo Scientific). Brain sections were cover slipped semi-dry in ProLong Gold Antifade Mountant (Life Technologies) or Fluorescence Mounting Medium (Dako).

Human samples were immunohistologically stained as follows: after antigen retrieval and H_2O_2 quench, sections were incubated in a primary antibody for 1 hour at room temperature. The following primary antibody was used: rabbit anti-DCX (1:3000, Abcam). Visualization was performed using the Menarini Diagnostics X-Cell DAB kit (MP-XCPDAB-U100) following the outlined protocol. All washes were done in Tris-buffered saline (TBS) buffer pH 7.6.

2.6. Microscopy, visualization, and image processing

For qualitative and quantitative microscopic analysis of mouse tissue, confocal laser scanning microscopy was

performed using a LSM 700 and LSM 710 from Zeiss. Representative images were taken as z-stack image from the stained sections. Orthogonal projections (maximum intensity) of the images were created and depicted in respective false colors using Zen 2012 blue edition software. For 3D reconstruction, images were processed at the LSM 710 using the Zen 2011 SP7 (black) software. Images were generated using the 3D tool with surface representation function, and each staining was depicted in respective false colors. Representative images of human DCX-stained samples were taken using a Nikon Eclipse E600 microscope and the NTS Elements Imaging Software (version 4.30.01).

2.7. Western blot analysis

For protein analysis, brains from 13-month-old APP-PS1 and littermates (n = 4/group) were extracted, and the hippocampus and cortex were dissected from one hemisphere per animal. Cortex and hippocampus regions were immediately frozen on dry ice and stored for further processing at −80°C. Brain regions were homogenized using an electric homogenizer pestle in 500 μL radioimmunoprecipitation assay buffer (50 mM Tris-HCl pH 7.4, 1% NP-40 [Sigma], 0.25% Na-deoxycholate [Sigma], and 150 mM NaCl, 1 mM EDTA), and protease (cOmplete, Roche) and phosphatase inhibitors (PhosStop, Roche). Afterward, lysates were manually dissociated using surgical needles of 20G and 27G size (Dispomed) to obtain a homogeneous sample solution. Samples were thoroughly vortexed, placed on an orbital shaker at 4°C for 30–60 min, and were then centrifuged for 20 min at 14,000 *g*. Supernatants were collected, and protein concentrations were calculated using Pierce BCA Protein Kit (ThermoFisher Scientific) following manufacturer's instruction. Total protein (7.5 μg) was denaturated for 5 min at 98°C in radioimmunoprecipitation assay buffer with sodium dodecyl sulfate sample loading buffer and loaded onto a Mini-Protean TGX stain-free precast gel (Bio-Rad). After standard sodium dodecyl sulfate–polyacrylamide gel electrophoresis, proteins were blotted onto a Mini-Format 0.2 μm nitrocellulose membrane using the Trans-Blot Turbo System (Bio-Rad) according to manufacturer's instructions. Afterward, the membranes were washed in TBS-T (TBS with 0.1% Tween) for a total of three washes. Membranes were blocked for 1 h at RT with TBS-T containing 4% bovine serum albumin (Sigma) and incubated over night at 4°C with following primary antibodies: rabbit anti-DCX (1:1000, Cell Signaling) and mouse anti-β-actin (1:2000, Sigma). The next day, membranes were washed three times 10 min in TBS-T and incubated with following secondary antibodies for 2 h at RT: donkey anti-rabbit Alexa Fluor 488 and donkey anti-mouse Alexa Fluor 568 (1:1000, all Molecular Probes). After three times 10 min washes of TBS-T, fluorescence signals were detected using the Chem-iDoc Mp Imaging System (Bio-Rad).

ImageJ (1.44p) and the function "Analyze Gel" was used for quantitative analysis. The protein band of interest and the loading control were selected from every loaded sample, and the area under the signal peak was calculated. After manual background subtraction, the protein band densities were normalized to β-actin. In addition, the densities of APP-PS1 lysates were normalized to wild type (WT) lysates and expressed as relative density to control lysate in %.

2.8. Electron microscopy

For ultrastructure analysis, 13-month-old APP-PS1 mice and WT controls were perfused with 4% paraformaldehyde and 0.5% glutaraldehyde in 0.1 M PB. Brains were removed, and 50 μm sagittal sections were cut using a vibratome and stored in 0.1 M PB with 0.05% sodium azide. Sections with brain areas of interest were selected and preembedding 3,3′-Diaminobenzidine immunostaining was performed as already described [23]. As primary antibody, the rabbit anti-DCX (1:300, Cell Signaling) antibody was used and incubated over night at RT. After several washes in PBS, sections were incubated for 3 h with goat anti-rabbit biotinylated antibody (1:500, Vector). To increase staining signal, sections were incubated in Vectastain ABC Hrp Kit (Vector) for 1 h according to manufacturer's instructions. After three times 10 min washing in PBS, sections were transferred to 3,3′-Diaminobenzidin using the Peroxidase Substrate Kit (Vector) following manufacturer's instructions. Sections were rigorously washed and osmificated by incubating in 1% OsO_4 (Electron Microscopy Sciences) in 0.1 M PB for 1 h. Following three washes for 10 min in distilled water, sections were incubated in Uranyl Acetate Replacement Stain (Electron Microscopy Sciences) for 30 min. Sections were dehydrated by incubation in an increasing series of ethanol and transferred to propylenoxide (Electron Microscopy Sciences) before embedding in araldite durcupan (four component resin, Sigma) over night in aluminum foil cups at RT. On the next day, the slices were gently transferred to acetate slides (100 micron color laser printer film, 5 star office), covered with small amounts of araldite and coated with a second acetate slide and hardened in an oven at 60°C for 3 days. Regions of interest were cut out of the embedded sections, followed by removing one side of the acetate slide and glueing on an araldite durcupan block with cyanoacrylate adhesive (UHU). This protocol was performed with small modifications according to the research group of José-Manuel Garcia Verdugo [45,46]. After removing the acetate slides and careful trimming of the samples into a trapezial shape, semithin sections of 1–1.5 μm were generated using a Reichert Ultracut S ultramicrotome (Leica). Semithin sections were transferred to object slides and were stained with 1% Toluidine blue for orientation. After identification of stained cells, ultrathin sections of 70 nm were directly cut using a diamond knife (Diatome). Sections were stretched with chloroform and subsequently collected with 75 mesh copper grids of 3 mm

diameter coated with 0.2% Formvar solution. Grids were dried and analyzed using a Zeiss Leo 910 electron microscope with an integrated Zeiss 906 TRS USB camera. The utilized software was ImageSP, version 1.2.4.29 from TRS & Sys Prog.

2.9. Qualitative and quantitative analysis of immunohistological data

For qualitative image analysis, amyloid plaques in the cortex, corpus callosum, and hippocampus from 10- to 13-month-old APP-PS1 animals were analyzed. Quantitative analysis of mean particle size and percentage area of staining was performed in 13-month-old APP-PS1 and age-matched WT littermates. For each animal, four fields of view in the cortex and hippocampus were photographed as z-stack at 40× magnification using a confocal laser scanning microscope (n = 3/group). Images were analyzed using ImageJ software (1.44p). For every image, maximum intensity projections were generated, and the threshold for each representative staining was manually set. The number of particles (bigger than 1 μm^2) and the particle areas [μm^2] were calculated for each staining using the ImageJ tool "Analyse particles". The total tissue area [in μm^2] of each image was calculated, and the % area (area of stained particles/field of view) was calculated.

Light microscopic analysis of human brain tissue was done as follows: images were captured at ×100 magnification, three from each region of interest: dentate gyrus, entorhinal cortex, and the CA1 and CA2 of the hippocampus, using a Zeiss Axio Scope A1 microscope with an Infinity 2 camera attached and using the Infinity 2-1C imaging software. Image analysis was performed by Image Pro Analyzer, version 6.3 software blind to disease state. The area of interest was identified, and positive staining was highlighted. Measurements for area, per area, and integrated optical density were taken for statistical analysis. All statistical analyses were done using GraphPad Prism.

2.10. Statistical analysis

Statistical analysis was performed using GraphPad Prism (GraphPad Software, version 5-7). Outliers were identified by Grubb test analysis (https://graphpad.com/quickcalcs/Grubbs1.cfm). Values between two groups were compared by the two-tailed unpaired Student's *t*-test with or without Welch's correction for normally distributed data. Two-way analysis of variance with Bonferroni post hoc test was performed for learning curve analysis of the MWM data. *P* values of $P < .0001$ (****) and $P < .001$ (***) were considered most significant, $P < .01$ (**) highly significant, and $P < .05$ (*) significant. Values were expressed as mean ± standard deviation or mean ± standard error of the mean.

3. Results

3.1. DCX-immunoreactive cells cluster at amyloid-β plaques in mouse brains and in human AD brain specimen

By analyzing amyloid plaque pathology in the cortex and hippocampus of 3-, 10-, and 13-month-old APP-PS1 animals, we recognized the presence of plaque-associated DCX-immunoreactive cells. These cells appeared with the onset of amyloid-β plaque deposition. Whereas, 3-months-old APP-PS1 animals were mostly devoid of amyloid-β plaques, 10- and 13-month-old animals already showed severe plaque pathology in hippocampal and cortical brain regions (Fig. 1A and 1B).

Interestingly, we observed increased DCX immunoreactivity clustered at these amyloid deposits (Fig. 1A and 1B). Three-month-old APP-PS1 animals did barely show any DCX immunoreactivity outside the neurogenic niches in cortical or hippocampal brain regions; however, increased DCX-positive staining was observed in cells surrounding cortical and hippocampal plaques of 10- and 13-month-old APP-PS1 animals (Fig. 1A and 1B). To test the specificity of the DCX antibody, appropriate negative controls were performed: omitting of primary antibody (Fig. 1C) and staining with an isotype control antibody (Fig. 1C′) to detect the level of nonspecific background signal. In addition, we proved the specificity of the DCX antibody used in this study, by staining DCX-KO brain tissue. The KO tissue did not show any staining in the dentate gyrus of the hippocampus (Fig. 1C″) or in any other brain region of DCX-KO animals.

To confirm the DCX protein expression in the APP-PS1 brain, we isolated proteins from the hippocampus and cortex of 13-month-old WT and APP-PS1 animals and performed Western blot analysis. In accordance with the immunohistochemistry data, the Western blot analysis showed increased amounts of DCX protein in the cortex of aged APP-PS1 animals compared with WT (Fig. 1D and 1E). This difference in DCX protein expression was not detected in hippocampal lysates, most likely due to the fact that the adult hippocampus expresses already high levels of DCX protein and that the further increase due to plaque-associated elevation of DCX expression might not be detected by Western blotting (Fig. 1D and 1E). Alternatively, a reduced level of hippocampal neurogenesis at this stage might cover the elevation of plaque-associated DCX protein levels.

Next, we investigated whether the appearance of DCX cells clustering around amyloid plaques was specific for the APP-PS1 mouse model or whether this was a more general phenomenon related to amyloid plaque pathologies. In all additional transgenic AD animal models tested at stages with advanced amyloid pathology, that is, the APP-Lon/Swe (11 months old) the APP-SDI (12 months old) and the Tg2576 (18 months old), DCX-immunoreactive cells were present at sites of amyloid deposits (Fig. 1F). Moreover,

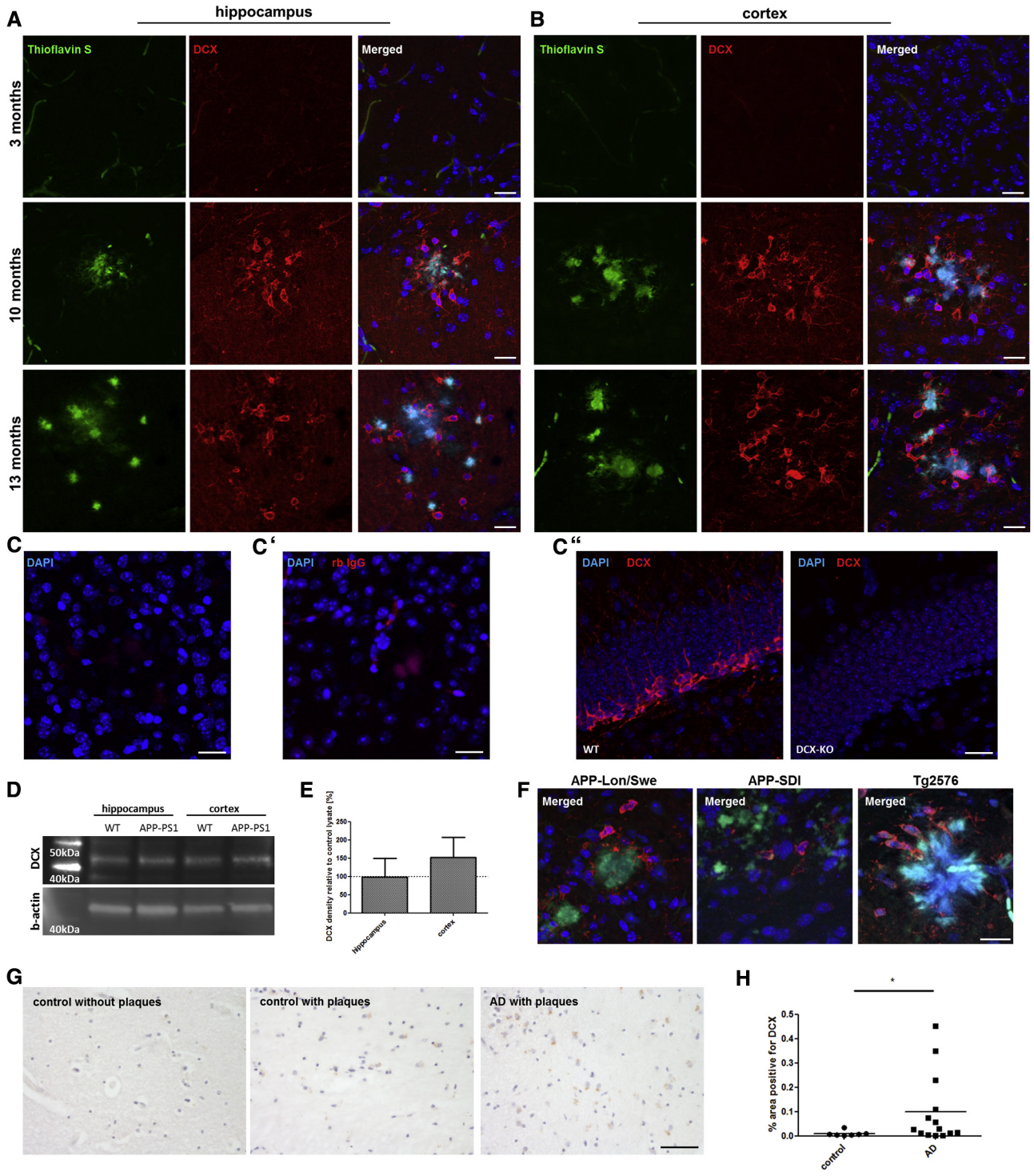

Fig. 1. Increased DCX immunoreactivity and protein expression at sites of amyloid deposits in brains of transgenic AD animals and human AD specimen: DCX-immunoreactive cells (red) were detected at sites of amyloid deposits (Thioflavin S, green) in the hippocampus (A) and cortex (B) of transgenic APP-PS1 animals with advanced plaque pathology. Three-month-old APP-PS1 animals were devoid of amyloid-β plaques and did barely show DCX-immunoreactive cells outside the neurogenic niche, whereas 10- and 13-month-old animals, with already severe plaque load, showed clustering of DCX-positive cells around amyloid plaques. Antibody staining and specificity were tested with appropriate negative controls, as omitting of primary antibody (C), staining with a rabbit IgG isotype control (C′) and staining of DCX-KO tissue (C″). (D) DCX protein expression was analyzed by Western blot using brain lysates from 13-month-old APP-PS1 compared with WT mice (n = 4/group). (E) DCX protein was increased in the cortex of APP-PS1 animals compared with WT animals, shown here as DCX density relative to control lysate (100%). (F) DCX-immunoreactive cells were detected in brains of various AD mouse models as the APP-Lon/Swe, APP-SDI and the Tg2576 (DCX in red, Thioflavin S in green). (G) Analysis of human postmortem brain samples revealed increased immunoreactivity for DCX in the hippocampus of AD specimen and controls with plaque pathology compared with controls without plaques. (H) Percentage area of staining for DCX was significantly increased in hippocampal CA1 brain region of human AD specimen compared with controls (* = $P < .05$, scatter

the analysis of human AD brain samples revealed increased DCX staining in hippocampus AD samples with plaques compared with control samples without any amyloid plaques (Fig. 1G). Furthermore, DCX staining was prominent in hippocampal brain structures of control samples, that is, clinically nondemented, with a detectable amount of plaque pathology (Fig. 1G). Semi-quantitative analysis revealed that the percentage area for DCX staining was significantly increased in human CA1 hippocampus regions of AD specimen compared with controls (Fig. 1H).

3.2. Two different DCX expressing cell types cluster at amyloid plaques in brains of APP-PS1 mice

We first hypothesized that the plaque-associated DCX cells might be of neurogenic origin. Therefore, we stained for markers of cell proliferation (proliferating cell nuclear antigen), stem and progenitor cells (Nestin, SOX2, PSA-NCAM), oligodendrocytes (Olig2), astrocytes (GFAP), and neurons (NeuN). However, none of these markers (except proliferating cell nuclear antigen) co-localized with the plaque-associated DCX cells (data not shown, see Table 1), suggesting that these cells were not of neurogenic origin. Surprisingly, however, the DCX-positive staining at sites of amyloid deposition in APP-PS1 animals highly co-localized with the microglia marker Iba1 (Fig. 2A). Interestingly, in areas with almost no amyloid deposits, microglia did barely, if at all, express DCX (Fig. 2A, rectangle). However, microglia directly located at sites of the amyloid plaques were observed as highly immunoreactive for DCX (Fig. 2A, arrow) to the extent that all plaque-associated Iba1 cells were DCX positive. We further observed a second population of DCX-immunoreactive cells, which did not express Iba1 and hence represent a non-microglia population (Fig. 2A, arrowhead). To investigate whether some of these DCX+ cells could be infiltrating macrophages or other peripheral immune cells, we performed staining with the pan-leukocyte marker CD45. Remarkably, all amyloid plaque–associated DCX+ cells clearly co-localized with CD45 (Fig. 2B, asterisk). One fraction of these cells co-localized with Iba1 and showed only very faint expression for CD45 (see Fig. 2B, asterisk), while the other fraction lacked the expression of Iba1 but was highly positive for CD45 (Fig. 2B, arrow). Vice versa, all plaque-associated CD45-positive cells were DCX positive. These data suggest the presence of two different DCX-expressing cell populations, one with a microglia identity and one with a hematopoietic origin. In the following, we refer to the cells that lack Iba1 but show high expression of CD45 as CD45++/DCX+ population; the Iba1 positive but CD45 faintly expressing DCX-immunoreactive population is termed Iba1+/DCX+.

Next, we performed quantitative analysis of DCX, Iba1, and CD45 expressions in APP-PS1 brain sections. We analyzed the percentage area (area of stained particles or field of view) for each respective staining in cortical and hippocampal brain regions of 13-months-old APP-PS1 animals and compared age-matched WT littermates. We detected a significant increase in the percentage area for Iba1 and DCX staining in the cortex of APP-PS1 animals compared with WT littermates (Fig. 3A and 3C). DCX immunoreactivity in the cortex co-localized with Iba1+/CD45+ microglia (Fig 3A, insert). Analysis of the hippocampus revealed a significant increase in percentage area of DCX staining (Fig. 3B and 3D). Furthermore, strong CD45++ cells, negative for Iba1, were detected in the brain parenchyma as being highly positive for DCX (Fig. 3B, asterisk).

To analyze the DCX expression at sites of amyloid deposits in more detail, we analyzed the ultrastructure of cortical and hippocampal brain regions from APP-PS1 animals using immunoelectron microscopy. DCX immunoreactivity was detected at the inner side of the cell membranes in processes of microglia that were located at sites of amyloid plaques (Fig. 2C, red arrow). A second population of cells with very strong DCX staining, but a different morphology was detected (Fig. 2D). In this population, DCX staining was localized within the cytoplasm and at the cortical actin-rich cytoskeleton of these small cells with a round-shaped nucleus and pseudopod-like structures (Fig. 2D, red arrow). These cells were identified by their morphology and CD45 expression (Fig. 2B) as leukocytes.

To summarize, we demonstrated an increased expression of DCX in brains of AD mouse models with already advanced plaque pathology and documented the occurrence of DCX-immunoreactive cells at sites of amyloid-β plaques. These cells were identified as Iba1+ microglia and CD45+ cells with hematopoietic origin. Ultrastructure analysis revealed intracellular DCX expression in microglia located at sites of amyloid deposition and in cells with leukocyte-like morphology.

3.3. DCX-immunoreactive cells at sites of amyloid-plaques are positive for markers of phagocytosis and contain engulfed plaque material in APP-PS1 mice

Because DCX-immunoreactive cells were observed very close to the amyloid deposits and co-localized with the microglia marker Iba1, we investigated whether DCX might be involved in amyloid plaque clearance. Therefore, we stained for various markers known to be involved in phagocytosis such as the triggering receptor 2 expressed on myeloid cells (TREM2) and the lysosomal marker CD68. Indeed, strong co-localization of DCX with TREM2-positive cells

plot with mean). In A, B, C, C′, C″, F, DAPI was used as nucleus stain. Unpaired Student's *t*-test with Welch's correction was performed (H, control n = 7, AD n = 14). Scale: 20 μm (A, B, C, C′, C″, F) and 50 μm (G). Abbreviations: DCX, doublecortin; APP-PS1, APP Swedish PS1 dE9; AD, Alzheimer's disease; DAPI, 4′,6′-diamidino-2-phenylindole dihydrochloride hydrate.

Table 1
List of makers used to characterize the DCX-immunoreactive cells associated with amyloid plaques

Cell type/function	Marker	Description	Colocalization with DCX
Proliferation	PCNA	Proliferating cell nuclear antigen, DNA clamp for replication	++
Stem and progenitor	Nestin	Neural stem cells (NSCs)	-
	Sox2	Neural stem and precursors, astrocytes, TF	-
	PSA-NCAM	Proliferating cells, neural cell adhesion molecule	-
Astrocyte	GFAP	NSCs and astrocytes, intermediate filament (IF)	-
Oligodendrocyte	Olig2	All oligodendrocytes, TF	-
Neuron	NeuN	Mature neuron, neuronal nuclei protein	-
Microglia	Iba1	Microglia, inflammation	+++
Phagocytosis	CD68	Macrophages, phagocytosis marker	+
	TREM2	Triggering receptor 2 expressed on myeloid cells	++
Hematopoietic lineage	CD45	Leukocyte common antigen	+++
	B220	CD45 isoform mainly expressed on B-cells	-
	Ly6G	Myeloid differentiation antigen expressed on granulocytes	-
	CD169	Lectin-like receptor expressed by macrophages/monocytes	-
T-cells	CD3	T-cell coreceptor used as pan-T-cell marker	++
	CD4	Membrane glycoprotein expressed on helper T-cells	-
	CD8	Cell surface glycoprotein expressed on cytotoxic T-cells	++
	Foxp3	Transcriptional regulator expressed on regulatory T-cells	-

Abbreviations: DCX, doublecortin; PCNA, proliferating cell nuclear antigen; TF, transcription factor.

NOTE. Detailed IHC characterization was performed using markers for cell proliferation, stem and progenitor cells, astrocytes, oligodendrocytes, neurons, microglia, phagocytosis, and of the hematopoietic cell lineage. DCX-immunoreactive cells at sites of plaques were negative for markers of neural stem- and progenitor cells, astrocytes, oligodendrocytes or mature neurons. Most interestingly, DCX immunoreactivity colocalized with markers for cell proliferation (PCNA), microglia (Iba1), phagocytosis (TREM2, CD68), and with markers for the hematopoietic cell lineage (CD45, CD3, and CD8).

NOTE. Few (+), moderate (++), and high (+++).

at sites of amyloid-β staining was detected (Fig. 4A). Also, we observed co-localization of DCX with CD68-positive microglia (Fig. 4B). In addition to the described co-localization of DCX with this phagocytosis-related marker, DCX-immunoreactive cells contained Thioflavin S-positive material in their cytoplasm (Fig. 4C). Moreover, high resolution images revealed that the DCX-positive cell cytoplasm reached toward the amyloid plaque deposits (Fig. 4D). These data strongly suggest that plaque-associated DCX cells participate in phagocytosing plaque material.

3.4. Plaque-associated CD45++/DCX+ immunoreactive cells are CD3+/CD8+ T-cells

We further tried to identify the CD45++ hematopoietic DCX-immunoreactive cell population in the APP-PS1 mouse brain in more detail by using various markers of the hematopoietic cell lineage (for details see Table 1). The CD45++/DCX+ cell population in the brain of APP-PS1 did not co-localize with markers of B-cells, granulocytes, or monocytes (data not shown). However, we found DCX-immunoreactive CD3+ T-cells in the brains of APP-PS1 animals (Fig. 5A). Those T-cells were randomly distributed in the brains, some were associated with vessels, but some were directly located at sites of amyloid deposition. Because regulatory T-cells (Foxp3+) and CD4+ T-cells were described to enter mouse brains with massive neurodegeneration and brains of AD animal models [13,47], we tested for CD4 and Foxp3 expression in the DCX+/CD3+ T-cell population. None of these markers were expressed by the CD45++/DCX + cell population. However, the majority of DCX-immunoreactive cells were positive for the T-cell marker CD8 (Fig. 5B, insert). Confocal imaging and 3D surface representation of high magnification images revealed that many of these DCX-immunoreactive CD8+ cells were closely attached to DCX+/Iba1+ microglia (Fig. 5C).

In summary, we detected DCX-immunoreactive cells at sites of amyloid-deposition in APP-PS1 animals. We identified two subpopulations of these cells: one population represents an Iba1+ microglia population immunoreactive for DCX, expressing markers for phagocytosis and with incorporated amyloid deposits. A further subpopulation of DCX-immunoreactive cells was positive for the T-cell marker CD3 and was characterized as a CD8-positive T-cell population most likely entering the brain and highly interacting with microglia.

4. Discussion

We employed a broadly used mouse model for AD, the APP-PS1 mouse model, which is well described to develop a variety of human hallmarks for AD pathology. The APP-PS1 mouse model starts to form amyloid-plaque deposits from 3–4 months of age [23,48–50] and along disease progression, it develops reactive astrogliosis [51], microgliosis or microglia activation [52,53], synaptic loss [54], changes in synaptic long-term potentiation [55], and even modest neuronal loss adjacent to plaques [56]. These changes in brain structure and function lead to a decline in cognitive performance of these mice, tested in several cognitive behavior tasks [55,57]. Indeed, we confirmed impaired

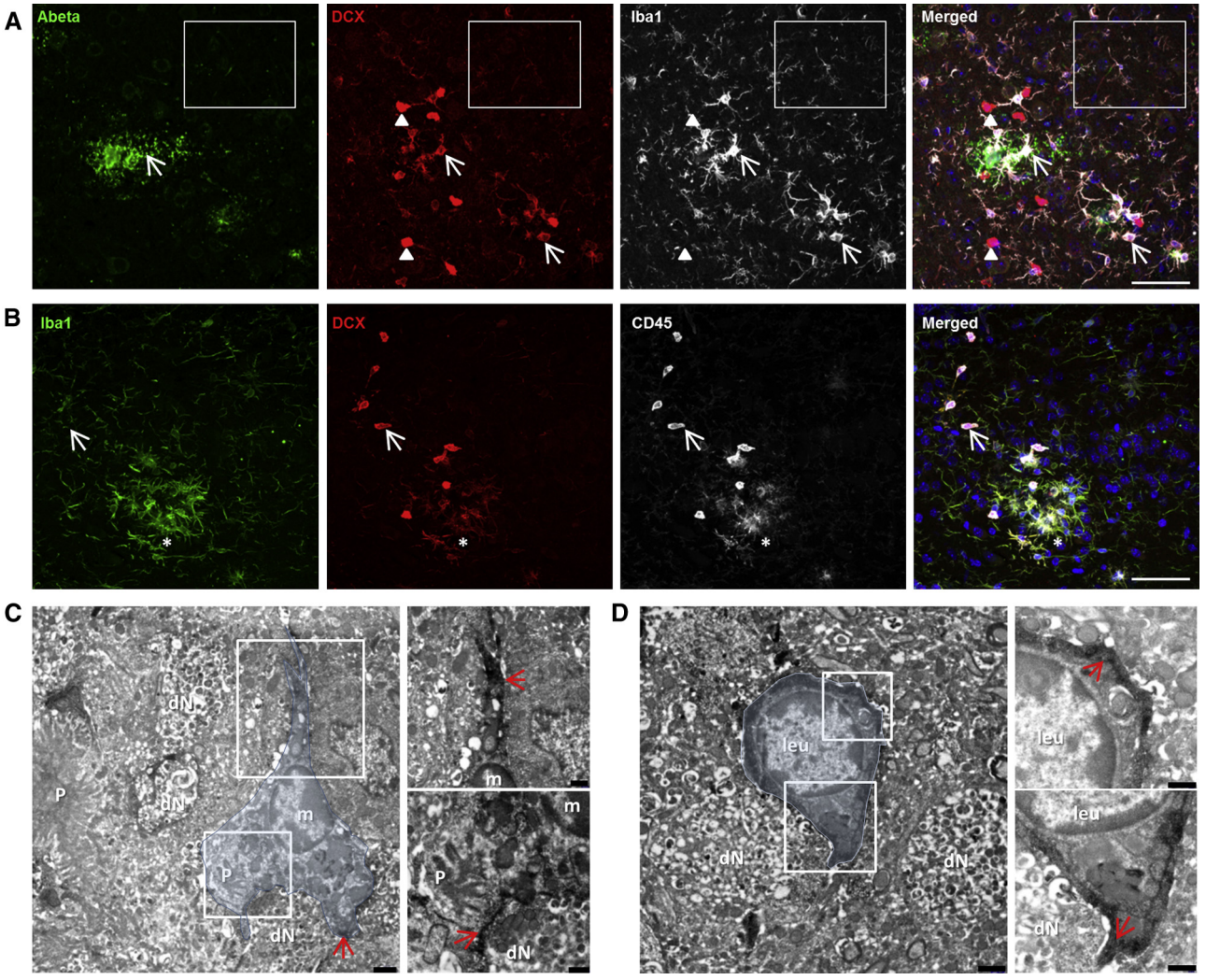

Fig. 2. DCX in microglia and hematopoietic cells at sites of cortical and hippocampal amyloid plaques in APP-PS1 mice: DCX immunoreactivity strongly colocalized with the microglia marker Iba1 (A). Microglia close to the amyloid plaques showed DCX expression (arrow), whereas microglia in areas with no amyloid deposition were barely positive for DCX (rectangle in A). Furthermore, a subpopulation of DCX-immunoreactive cells lacking the expression of Iba1 was detected (A, triangle). Using the pan-leukocyte marker CD45 for further characterization of the DCX-immunoreactive population revealed two distinct DCX cell types at sites of amyloid deposition: a DCX+/Iba1+/CD45+ microglia (asterisk) and a DCX+/Iba1−/CD45++ population (B, arrow). (C) Ultrastructure analysis of DCX-DAB immunostained APP-PS1 brains showed intracellular DCX protein localization in microglia (m) and leukocyte-like cells (leu) at sites of neuritic cortical and hippocampal amyloid plaques (P). Microglia at sites of an amyloid core and dystrophic neurites (dN), containing electrodense laminar bodies, showed intracellular DCX expression in their processes and in the cytoplasm along their inner cell membrane (C, red arrows). In addition, strong polarized DCX expression lining the inner cell membrane was observed in leukocyte-like cells of round shape, with pseudopod-like processes (D, red arrows). In A, B DAPI was used as nucleus stain. Scale: 50 μm (A, B), 1 μm (C, D) and 500 nm (C, D inserts). Cell bodies and borders were visualized in blue. Abbreviations: DCX, doublecortin; APP-PS1, APP Swedish PS1 dE9; Abeta; amyloid β; DAB, 3,3′-Diaminobenzidine.

learning and memory function in APP-PS1 mice using MWM test for spatial learning and memory (Supplementary Fig. 1). Animals were trained to find a water-submerged platform over a time period of 5 days, and the total distance the animals traveled to find the platform was analyzed. APP-PS1 animals significantly traveled higher distances to reach the platform compared with age-matched control animals indicating reduced learning function (Supplementary Fig. 1A and 1B). Spatial memory analysis after removal of the platform on day 6 revealed decreased memory functions in APP-PS1 animals compared with age-matched controls (Supplementary Fig. 1C). Nevertheless, the APP-PS1 mouse has its limitations as a model for AD. Obviously, spatial learning and memory is only one of the plethoras of cognitive dysfunctions AD patients are suffering from, and therefore, data derived from experiments with APP-PS1 animals should not be overinterpreted. Also, APP-PS1 mice do not develop NFTs by hyperphosphorylation of the tau protein, which is observed in the brains of many AD patients [37]. Finally, the APP-PS1 model represents one of the genetic and familial forms of AD and not the much more frequent sporadic forms.

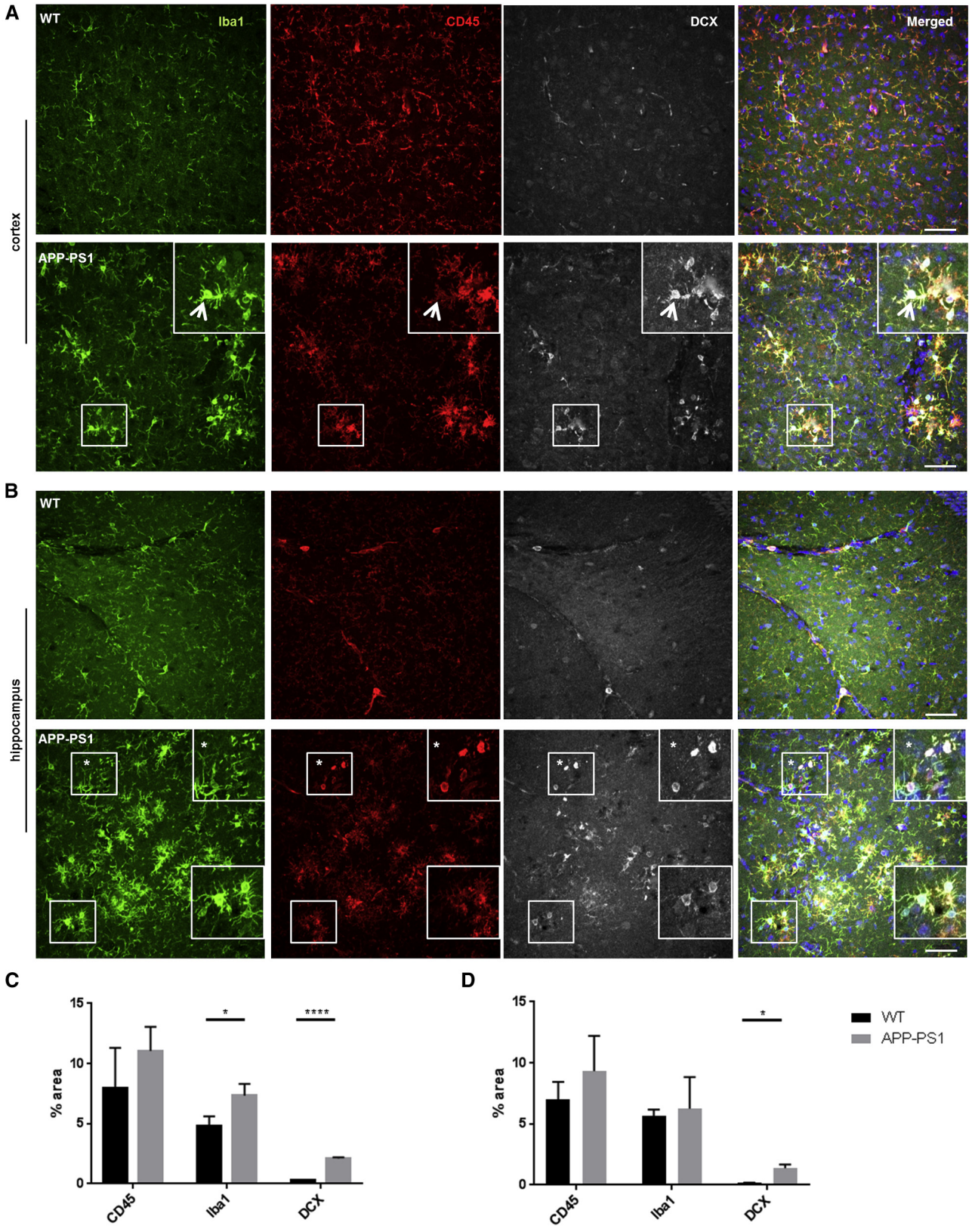

Fig. 3. Semi-quantitative analysis of Iba1, CD45, and DCX expression in APP-PS1 mouse brains: Microglia marker Iba1, pan-leukocyte marker CD45, and DCX staining in cortical (A) and hippocampal (B) brain regions of 13-month-old APP-PS1 mice. The percentage area (area of stained particles per field of view) of each respective staining was calculated using ImageJ software. APP-PS1 mice showed a significant increase in percentage area for Iba1 and DCX staining in the cortex compared with WT littermates (C). DCX expression colocalized with Iba1+/CD45+ microglia (A, insert with arrow). Analysis of

Here, we identify and characterize DCX-immunoreactive cells outside the neurogenic niches at sites of amyloid deposition in the brains of transgenic amyloid-plaque mouse models and in human AD specimen. The plaque-associated DCX cells were of nonneurogenic origin, as they lacked the expression of stem or progenitor cell markers and those of neuronal and glial cells (see Table 1). This is essential knowledge, as DCX is generally used as a marker for young immature neurons and for neurogenesis [21,22]. Thus, elevated DCX expression in brains with neurodegeneration outside of the neurogenic niches could easily be misinterpreted as enhanced neurogenesis. There were no obvious signs of potential migration of these cells from the neurogenic niches, instead they were highly proliferative (data not shown) and clustered at plaques in the transgenic animal models. This may lead to the assumption that at least some of these cells were generated locally. The plaque-associated DCX+ cells were identified as immune cells, more specifically as Iba1+ microglia and as CD8+ T-cells. These two cell types appeared in close proximity to each other, suggesting that they might interact and modulate phagocytic and/or immune activities.

DCX is highly expressed in the developing brain, specifically in migrating or differentiating neurons [58,59]. In the adult organism, its expression is mainly confined to neuronal precursor cells and young immature neurons in the neurogenic niches of the dentate gyrus and of the subventricular zone of the lateral ventricle [21,22]. There is very little evidence for DCX expression in the adult uninjured brain in cells outside the neurogenic regions, and if it appears then, that DCX expression in such areas is confined to cells of neurogenic origin. For example, in the piriform cortex, a pool of neurons with an immature phenotype retains DCX expression in the adult [60], and it is thought that such immature DCX neurons might provide the brain circuitry with increased plasticity [61,62]. Interestingly, cortical DCX expression in nonneurogenic regions is unaffected by age or by neurogenesis-inhibiting interventions such as radiation [63].

In animal models of stroke, leptomeningeal cells express DCX, and these cells might contribute to repair processes [64]. Also, after stroke, the production of DCX cells in the subventricular zone is increased, and DCX-positive cells migrate toward the lesion site [65]. Besides immature neurons, GFAP-positive astroglia have been shown to express DCX after an ischemic lesion [66]. Furthermore, DCX expression was described in oligodendrocyte precursor cells of healthy rodent brains [67]. Taking into account that levels of adult neurogenesis, that is, levels of DCX + neuronal progenitors, correlate with cognitive behavior in rodent animal models [68], the nonneurogenic DCX protein expression detected along amyloid pathology has to be carefully interpreted. At least, up to now, there is no correlation between nonneurogenic DCX cells in the brain and cognitive outcomes. Nevertheless, one possible interpretation of this might be a beneficial process allowing cellular plasticity and involvement in regeneration rather than being detrimental. To address the question whether nonneurogenic DCX-positive cells are generally present in rodent models for neurodegenerative diseases, we additionally analyzed DCX expression in a Lewy body dementia mouse model with severe α-synucleinopathy in the brain [34]. We did not observe DCX expression in these transgenic mice other than in the hippocampal neurogenic niche, and there was no co-localization with microglia marker (Supplementary Fig. 2). Therefore, it is more likely that the herein described nonneurogenic DCX expression is specific for amyloid pathology; however, this would need further investigations. Nevertheless, if so, this harbors the possibility of the future use of DCX to stratify AD brains in neuropathology.

The microglia fraction of the plaque-associated DCX cells co-expressed the microglia markers Iba1, CD68, and TREM2, suggesting that these cells are phagocytic cells. Indeed, they showed incorporated amyloid deposits in their cell soma. Interestingly, non–plaque-associated microglia as well as microglia in wild type mice did barely show any DCX immunoreactivity. This might be an explanation for the fact that DCX was so far never described in microglia of the adult brain. Nevertheless, there is evidence that microglia do express DCX under certain circumstances. A RNA sequence database on embryonic and adult-isolated microglia [69] reveals that microglia during development do express DCX mRNA at considerable amounts compared with all genes (Fragments Per Kilobase Million 46), but they lose DCX expression during postnatal stages (http://web.stanford.edu/group/barres_lab/cgi-bin/geneSearchMariko.py?geneNameIn=DCX).

Also, a transcriptome analysis of amoeboid microglia versus ramified microglia isolated from the corpus callosum of rat brains revealed expression of DCX in microglia. The DCX gene was within the top 25 highly expressed genes in amoeboid microglia but was not expressed in ramified microglia. At the protein level, the authors demonstrated that amoeboid microglia showed positive immunoreactivity for DCX [70]. The function of DCX in developmental or amoeboid microglia is unclear, but as DCX is a microtubule-associated protein involved in neuronal migration [71,72], it might as well modulate migration and motility of microglia. Alternatively, DCX might be involved in intracellular processes such as phagocytosis. Phagocytosis is a key function of microglia and involves high motility and

the hippocampus revealed a significantly increased percentage area of DCX staining in APP-PS1 animals compared with WT (D). Furthermore, strongly CD45++ cells negative for Iba1 were detected in the brain parenchyma being highly positive for DCX (asterisk in B). DAPI was used as nucleus stain. Unpaired Student's *t*-test (* = $P < .05$, **** = $P < .0001$, mean ± SD) with or without Welch's correction (n = 3/group) for each staining was performed (C, D). Scale: 50 μm (A, B). Arrows indicate colocalization. Abbreviations: DCX, doublecortin; APP-PS1, APP Swedish PS1 dE9; SD, standard deviation.

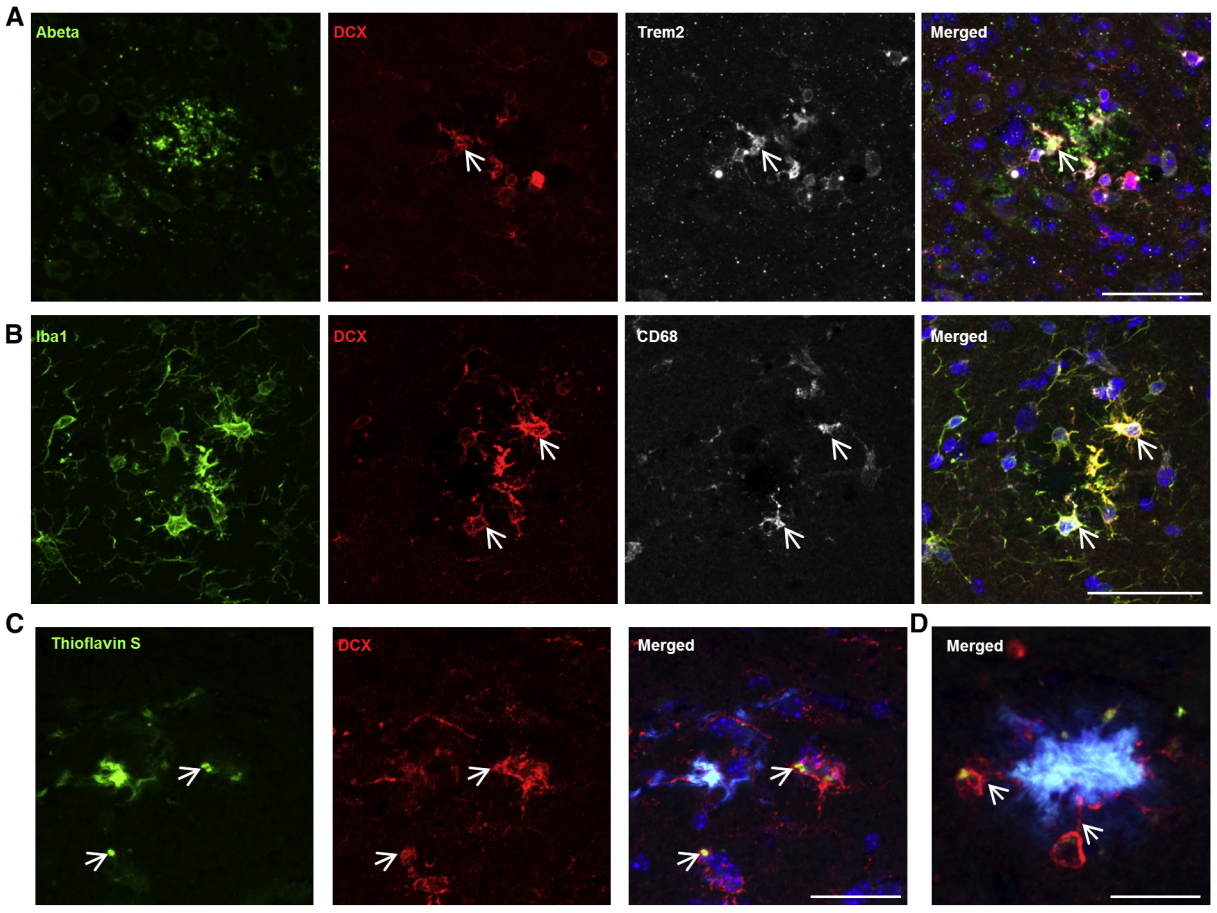

Fig. 4. DCX+ microglia are phagocytotic: Strong colocalization of DCX with the microglia phagocytosis marker TREM2 (A, arrow) and with the lysosomal marker CD68 (B, arrow) at sites of amyloid-β deposition. DCX-immunoreactive cells closely attached to the amyloid-plaque had Thioflavin S positive particles incorporated into their cell soma (C, arrow). High-resolution images revealed DCX-positive cell cytoplasm reaching toward amyloid plaques (D, arrow). DAPI was used as nucleus stain. Scale: 50 μm (A, B), 20 μm (C, D). Arrows indicate colocalization. Abbreviations: DCX, doublecortin; Abeta; amyloid β.

plasticity of the intracellular cytoskeleton coordinated by various receptor complexes on the microglia cell surface [9]. DCX might play an essential role in cytoskeletal reorganization specifically in microglia associated with the amyloid-β plaques. Regardless of a putative function of DCX in this process, the morphology and location, as well as the expression of the phagocytosis markers TREM2 and CD68, and the presence of amyloid plaque material in the DCX cells strongly suggests that they have phagocytic activity and that they contribute to amyloid plaque clearance. The role of TREM2 and of microglia-mediated phagocytosis in AD pathogenesis is evident, as human genetic studies showed a higher risk to develop AD with certain TREM2 variants [73]. Besides TREM2, the co-localization of the DCX cells with CD68 also points toward a critical role in phagocytosis, as CD68 is expressed in lysosomal vesicles [74,75].

The DCX immunoreactivity was not limited to the microglia cell population at sites of amyloid plaques. We identified a specific hematopoietic T-cell population present in the brain of APP-PS1 animals, which was positive for DCX. Assuming that these cells infiltrated the brain from the periphery, we also analyzed peripheral immune organs, for example, spleen and bone marrow from adult mice, and surprisingly found high DCX immunoreactivity in T-cell–rich areas of this tissue (Supplementary Fig. 3). We used various markers of the hematopoietic cell lineage to characterize these cells in the brain of APP-PS1 animals and detected mainly CD8+ DCX-immunoreactive T-cells that were in direct contact with microglia. The existence of two subpopulations of nonneurogenic DCX+ cells is fascinating and might be explained by their cellular function: microglia as already discussed previously have to be highly motile for phagocytosis, and T-cells have to form and change their cytoskeleton depending on their activity status [76,77]. Both functions involve cytoskeleton reorganization and might therefore involve the DCX protein.

The occurrence of peripheral immune cells, specifically T-cells, in the brain and their functional role and interaction

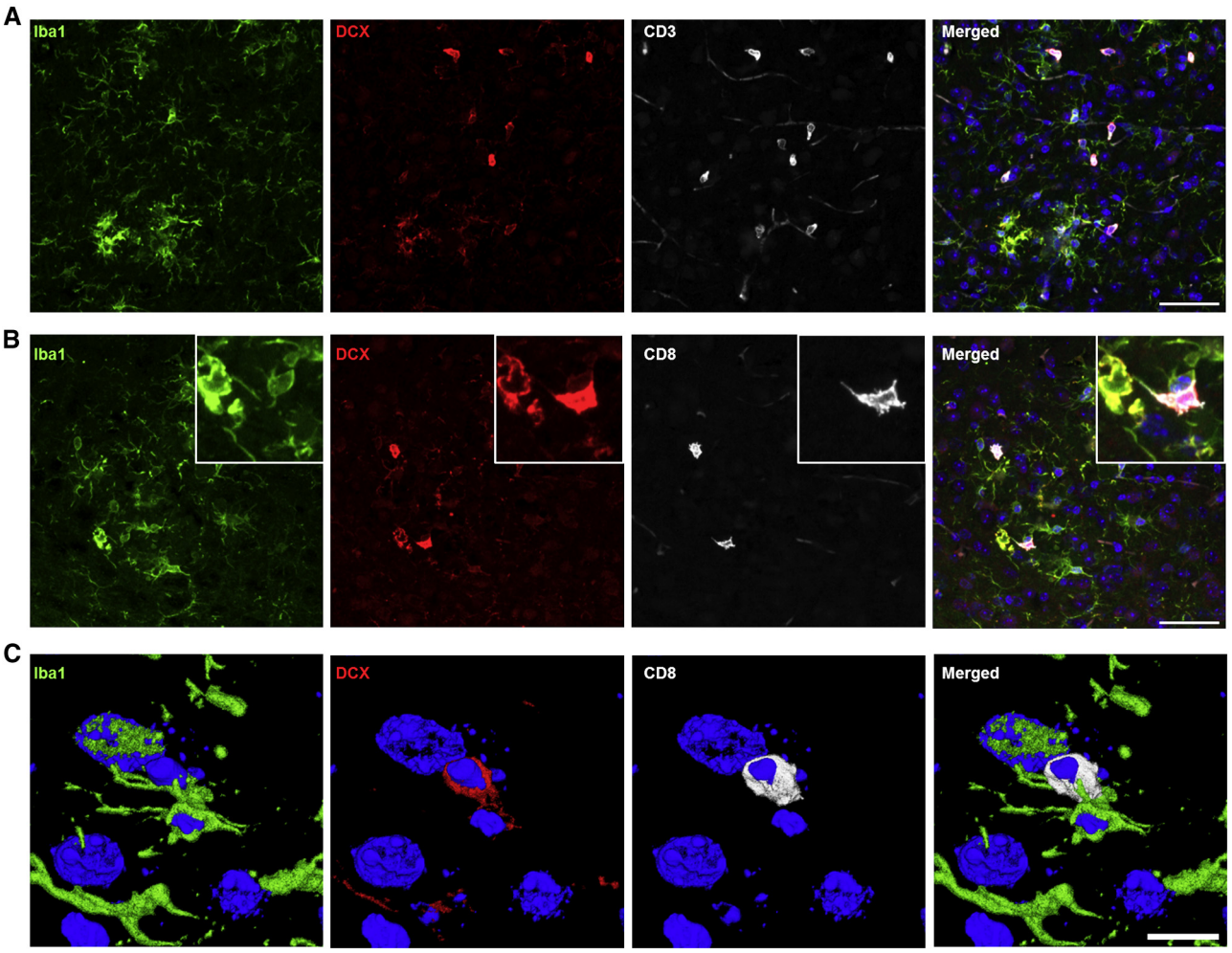

Fig. 5. DCX+/CD8+ T-cells in APP-PS1 mouse brains: (A) DCX-immunoreactive cells that lack the microglia marker Iba1 were highly positive for the T-cell marker CD3. Most interestingly, in the brain, no colocalization with Foxp3 or CD4 was detected (data not shown). (B) The majority of T-cells did express CD8 and were therefore identified as natural killer T-cells present in the brain parenchyma of APP-PS1 animals. These DCX+/CD8+ T-cells were often located very closely to microglia suggesting a strong interaction of these two cell populations (B, insert). High magnification images and 3D surface representation showed detailed DCX colocalization with CD8 and Iba1-positive cells (C). DAPI was used as nucleus stain. Scale: 50 μm (A, B), 10 μm (C). Abbreviations: DCX, doublecortin; APP-PS1, APP Swedish PS1 dE9.

with brain resident glial cells is currently discussed, and increased T-cell homing into the healthy aged brain has been reported [11,12]. Although the increased occurrence of T-cells in the brains of patients with autoimmune diseases such as multiple sclerosis is well documented, the evidence of T-cells in chronic neurodegenerative disease such as AD is less [78]. The occurrence of T-cells in the brain was first reported in human AD postmortem brain biopsies in 1988 [79]. Elevated numbers of T-cells in the brains of amyloid plaque mouse models has further been documented in several transgenic AD mouse models [13]. This, of course, raises the question whether T-cells might have a modulatory activity, ameliorating or worsening AD pathology [14]. Whereas, studies on regulatory T-cells (Tregs) report on a beneficial function of T-cells by slowing down disease progression and modulating microglia responses to amyloid-β deposits [80], others report about detrimental effects of Tregs in AD. For example, while in one study, depletion or inhibition of Tregs reversed the cognitive deficits in an AD animal model [47], the genetic ablation of T-, B-, and natural killer cells in a 5XFAD AD mouse model (Rag-5xfAD) revealed a twofold increase in amyloid-β plaque pathology and exacerbated neuroinflammation. Conversely, bone marrow transplantation in these mice again reduced AD pathology [81].

We summarized our findings in a hypothesis model for T-cell microglia interaction in amyloid plaque-diseased brains (Fig. 6). It will be essential to uncover the functional role of the different T-cell subpopulations in the brain along AD pathology. In particular, research on these cells and their interactions with central nervous system resident cells such as microglia, neurons, and others might identify new therapeutic targets in future. So far, the functional characterization of these cells is very limited, and their

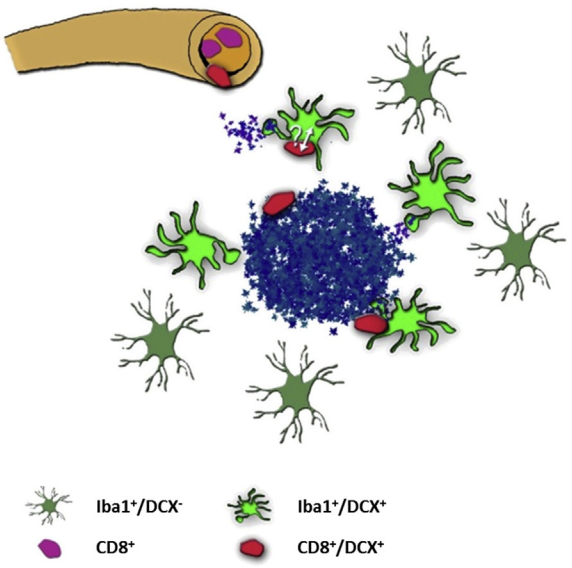

Fig. 6. Schematic representation of the T-cell microglia interaction showing DCX+ microglia and DCX+/CD8+ T-cells associated to amyloid plaques. With increased amyloid plaque deposition activated microglia cluster at sites of the amyloid plaques and express the microtubule-associated protein DCX (Iba1+/DCX+, light green). Via blood vessels (orange) DCX+ T-cells (red) were observed to infiltrate the brain parenchyma and closely attached with brain resident microglia, presumably modulating immune cell functions. Abbreviation: DCX, doublecortin.

interactions with the brains resident glial cells are not fully understood. We confirmed our main findings in several other amyloid plaque models and even in human AD brains or brains with plaque pathology, considering our finding relevant for the broad AD field.

Acknowledgments

The authors thank the microscopy core facility of SCI-TReCS (Spinal Cord Injury and Tissue Regeneration Center Salzburg), Pia Zaunmair, and Stephanie Schwartz for her support with the animal work. The authors are grateful to K. Hsiao-Ashe and for S.R. for providing Tg2576 mice. Furthermore, we thank Fiona Francis for providing DCX-KO tissue. This work was supported by the FWF Special Research Program (SFB) F44 (F4413-B23) "Cell Signaling in Chronic CNS Disorders", by the FWF Hertha-Firnberg Postdoctoral programme n° T736-B24, by the State Government of Salzburg, Austria, (Stiftungsprofessur, and 20204-WISS/80/199-2014), through funding from the European Union's Seventh Framework Program (FP7/2007-2013) under grant agreements n° HEALTH-F2-2011-278850 (INMiND), n° HEALTH-F2-2011-279288 (IDEA), n° FP7-REGPOT-316120 (GlowBrain), by grants of the German Research Foundation (RO 2226/13-1) and by the German Federal Department of Education, Science and Technology (BMBF #01ED1501 B) within the JPND program CrossSeeds to S.R. Tissue for this study was provided by the Newcastle Brain Tissue Resource, which is funded in part by a grant from the UK Medical Research Council (G0400074) and by Brains for Dementia research, a joint venture between Alzheimer's Society and Alzheimer's Research UK.

Supplementary data

Supplementary data related to this article can be found at https://doi.org/10.1016/j.jalz.2018.02.017.

RESEARCH IN CONTEXT

1. Systematic review: The authors reviewed the literature using traditional (e.g., PubMed) sources and meeting abstracts and presentations. Doublecortin positive cells have been analyzed in AD and in amyloid plaque models of AD, however, always in the context of neurogenic niches. These relevant citations are appropriately cited.
2. Interpretation: Our findings led to an integrated hypothesis describing two populations of doublecortin expressing cells associated with plaques, that is, microglia and CD8 T-cells.
3. Future directions: Need to investigate the role of the two cell population in plaque pathology.

References

[1] Goedert M, Spillantini MG. A century of Alzheimer's disease. Science 2006;314:777–81.
[2] Selkoe DJ. Alzheimer's disease: genes, proteins, and therapy. Physiol Rev 2001;81:741–66.
[3] Philipson O, Lord A, Gumucio A, O'Callaghan P, Lannfelt L, Nilsson LN. Animal models of amyloid-beta-related pathologies in Alzheimer's disease. FEBS J 2010;277:1389–409.
[4] Hall AM, Roberson ED. Mouse models of Alzheimer's disease. Brain Res Bull 2012;88:3–12.
[5] Heneka MT, Carson MJ, El Khoury J, Landreth GE, Brosseron F, Feinstein DL, et al. Neuroinflammation in Alzheimer's disease. Lancet Neurol 2015;14:388–405.
[6] Wyss-Coray T. Inflammation in Alzheimer disease: driving force, bystander or beneficial response? Nat Med 2006;12:1005–15.
[7] Wyss-Coray T, Rogers J. Inflammation in Alzheimer disease-a brief review of the basic science and clinical literature. Cold Spring Harb Perspect Med 2012;2:a006346.
[8] Stalder M, Phinney A, Probst A, Sommer B, Staufenbiel M, Jucker M. Association of microglia with amyloid plaques in brains of APP23 transgenic mice. Am J Pathol 1999;154:1673–84.
[9] Fu R, Shen Q, Xu P, Luo JJ, Tang Y. Phagocytosis of microglia in the central nervous system diseases. Mol Neurobiol 2014;49:1422–34.
[10] Mosher KI, Wyss-Coray T. Microglial dysfunction in brain aging and Alzheimer's disease. Biochem Pharmacol 2014;88:594–604.
[11] Gemechu JM, Bentivoglio M. T Cell recruitment in the brain during normal aging. Front Cell Neurosci 2012;6:38.
[12] Ritzel RM, Crapser J, Patel AR, Verma R, Grenier JM, Chauhan A, et al. Age-associated resident memory CD8 T cells in the central

nervous system are primed to potentiate inflammation after ischemic brain injury. J Immunol 2016;196:3318–30.
[13] Ferretti MT, Merlini M, Spani C, Gericke C, Schweizer N, Enzmann G, et al. T-cell brain infiltration and immature antigen-presenting cells in transgenic models of Alzheimer's disease-like cerebral amyloidosis. Brain Behav Immun 2016;54:211–25.
[14] McManus RM, Mills KH, Lynch MA. T Cells-Protective or Pathogenic in Alzheimer's Disease? J Neuroimmune Pharmacol 2015; 10:547–60.
[15] Chuang TT. Neurogenesis in mouse models of Alzheimer's disease. Biochim Biophys Acta 2010;1802:872–80.
[16] Spalding KL, Bhardwaj RD, Buchholz BA, Druid H, Frisen J. Retrospective birth dating of cells in humans. Cell 2005;122:133–43.
[17] Altman J. Are new neurons formed in the brains of adult mammals? Science 1962;135:1127–8.
[18] Eriksson PS, Perfilieva E, Bjork-Eriksson T, Alborn AM, Nordborg C, Peterson DA, et al. Neurogenesis in the adult human hippocampus. Nat Med 1998;4:1313–7.
[19] Colucci-D'Amato L, Bonavita V, di Porzio U. The end of the central dogma of neurobiology: stem cells and neurogenesis in adult CNS. Neurol Sci 2006;27:266–70.
[20] Vivar C, van Praag H. Functional circuits of new neurons in the dentate gyrus. Front Neural Circuits 2013;7:15.
[21] Couillard-Despres S, Winner B, Schaubeck S, Aigner R, Vroemen M, Weidner N, et al. Doublecortin expression levels in adult brain reflect neurogenesis. Eur J Neurosci 2005;21:1–14.
[22] Brown JP, Couillard-Despres S, Cooper-Kuhn CM, Winkler J, Aigner L, Kuhn HG. Transient expression of doublecortin during adult neurogenesis. J Comp Neurol 2003;467:1–10.
[23] Unger MS, Marschallinger J, Kaindl J, Hofling C, Rossner S, Heneka MT, et al. Early changes in hippocampal neurogenesis in transgenic mouse models for Alzheimer's disease. Mol Neurobiol 2016;53:5796–806.
[24] Jankowsky JL, Slunt HH, Ratovitski T, Jenkins NA, Copeland NG, Borchelt DR. Co-expression of multiple transgenes in mouse CNS: a comparison of strategies. Biomol Eng 2001;17:157–65.
[25] Rockenstein E, Mallory M, Mante M, Sisk A, Masliaha E. Early formation of mature amyloid-beta protein deposits in a mutant APP transgenic model depends on levels of Abeta(1-42). J Neurosci Res 2001; 66:573–82.
[26] Daschil N, Obermair GJ, Flucher BE, Stefanova N, Hutter-Paier B, Windisch M, et al. CaV1.2 calcium channel expression in reactive astrocytes is associated with the formation of amyloid-beta plaques in an Alzheimer's disease mouse model. J Alzheimers Dis 2013;37:439–51.
[27] Davis J, Xu F, Deane R, Romanov G, Previti ML, Zeigler K, et al. Early-onset and robust cerebral microvascular accumulation of amyloid beta-protein in transgenic mice expressing low levels of a vasculotropic Dutch/Iowa mutant form of amyloid beta-protein precursor. J Biol Chem 2004;279:20296–306.
[28] Kniewallner KM, Wenzel D, Humpel C. Thiazine Red(+) platelet inclusions in Cerebral Blood Vessels are first signs in an Alzheimer's Disease mouse model. Sci Rep 2016;6:28447.
[29] Shah D, Praet J, Latif Hernandez A, Hofling C, Anckaerts C, Bard F, et al. Early pathologic amyloid induces hypersynchrony of BOLD resting-state networks in transgenic mice and provides an early therapeutic window before amyloid plaque deposition. Alzheimers Dement 2016;12:964–76.
[30] Hsiao K, Chapman P, Nilsen S, Eckman C, Harigaya Y, Younkin S, et al. Correlative memory deficits, Abeta elevation, and amyloid plaques in transgenic mice. Science 1996;274:99–102.
[31] Kappeler C, Saillour Y, Baudoin JP, Tuy FP, Alvarez C, Houbron C, et al. Branching and nucleokinesis defects in migrating interneurons derived from doublecortin knockout mice. Hum Mol Genet 2006; 15:1387–400.
[32] Masliah E, Rockenstein E, Mante M, Crews L, Spencer B, Adame A, et al. Passive immunization reduces behavioral and neuropathological deficits in an alpha-synuclein transgenic model of Lewy body disease. PLoS One 2011;6:e19338.
[33] Masliah E, Rockenstein E, Veinbergs I, Mallory M, Hashimoto M, Takeda A, et al. Dopaminergic loss and inclusion body formation in alpha-synuclein mice: implications for neurodegenerative disorders. Science 2000;287:1265–9.
[34] Rockenstein E, Mallory M, Hashimoto M, Song D, Shults CW, Lang I, et al. Differential neuropathological alterations in transgenic mice expressing alpha-synuclein from the platelet-derived growth factor and Thy-1 promoters. J Neurosci Res 2002;68:568–78.
[35] Rotheneichner P, Romanelli P, Bieler L, Pagitsch S Zaunmair P, Kreutzer C, et al. Tamoxifen activation of Cre-Recombinase has no persisting effects on adult neurogenesis or learning and anxiety. Front Neurosci 2017;11:27.
[36] Lagace DC, Whitman MC, Noonan MA, Ables JL, DeCarolis NA, Arguello AA, et al. Dynamic contribution of nestin-expressing stem cells to adult neurogenesis. J Neurosci 2007;27:12623–9.
[37] Braak H, Alafuzoff I, Arzberger T, Kretzschmar H, Del Tredici K. Staging of Alzheimer disease-associated neurofibrillary pathology using paraffin sections and immunocytochemistry. Acta Neuropathol 2006;112:389–404.
[38] Braak H, Braak E. Neuropathological stageing of Alzheimer-related changes. Acta Neuropathol 1991;82:239–59.
[39] Mirra SS, Heyman A, McKeel D, Sumi SM, Crain BJ, Brownlee LM, et al. The Consortium to Establish a Registry for Alzheimer's Disease (CERAD). Part II. Standardization of the neuropathologic assessment of Alzheimer's disease. Neurology 1991;41:479–86.
[40] McKeith IG, Dickson DW, Lowe J, Emre M, O'Brien JT, Feldman H, et al. Diagnosis and management of dementia with Lewy bodies: third report of the DLB Consortium. Neurology 2005;65:1863–72.
[41] Montine TJ, Phelps CH, Beach TG, Bigio EH, Cairns NJ, Dickson DW, et al. National Institute on Aging-Alzheimer's Association guidelines for the neuropathologic assessment of Alzheimer's disease: a practical approach. Acta Neuropathol 2012;123:1–11.
[42] Thal DR, Rub U, Orantes M, Braak H. Phases of A beta-deposition in the human brain and its relevance for the development of AD. Neurology 2002;58:1791–800.
[43] Marschallinger J, Sah A, Schmuckermair C, Unger M, Rotheneichner P, Kharitonova M, et al. The L-type calcium channel Cav1.3 is required for proper hippocampal neurogenesis and cognitive functions. Cell Calcium 2015;58:606–16.
[44] Schnell SA, Staines WA, Wessendorf MW. Reduction of lipofuscin-like autofluorescence in fluorescently labeled tissue. J Histochem Cytochem 1999;47:719–30.
[45] Gil-Perotin S, Alvarez-Buylla A, Garcia-Verdugo JM. Identification and characterization of neural progenitor cells in the adult mammalian brain. Adv Anat Embryol Cell Biol 2009;203:1–101, ix.
[46] Sirerol-Piquer MS, Cebrian-Silla A, Alfaro-Cervello C, Gomez-Pinedo U, Soriano-Navarro M, Verdugo JM. GFP immunogold staining, from light to electron microscopy, in mammalian cells. Micron 2012;43:589–99.
[47] Baruch K, Rosenzweig N, Kertser A, Deczkowska A, Sharif AM, Spinrad A, et al. Breaking immune tolerance by targeting Foxp3(+) regulatory T cells mitigates Alzheimer's disease pathology. Nat Commun 2015;6:7967.
[48] Garcia-Alloza M, Robbins EM, Zhang-Nunes SX, Purcell SM, Betensky RA, Raju S, et al. Characterization of amyloid deposition in the APPswe/PS1dE9 mouse model of Alzheimer disease. Neurobiol Dis 2006;24:516–24.
[49] Borchelt DR, Ratovitski T, van Lare J, Lee MK, Gonzales V, Jenkins NA, et al. Accelerated amyloid deposition in the brains of transgenic mice coexpressing mutant presenilin 1 and amyloid precursor proteins. Neuron 1997;19:939–45.
[50] Hamilton A, Holscher C. The effect of ageing on neurogenesis and oxidative stress in the APP(swe)/PS1(deltaE9) mouse model of Alzheimer's disease. Brain Res 2012;1449:83–93.

[51] Kamphuis W, Mamber C, Moeton M, Kooijman L, Sluijs JA, Jansen AH, et al. GFAP isoforms in adult mouse brain with a focus on neurogenic astrocytes and reactive astrogliosis in mouse models of Alzheimer disease. PLoS One 2012;7:e42823.
[52] Babcock AA, Ilkjaer L, Clausen BH, Villadsen B, Dissing-Olesen L, Bendixen AT, et al. Cytokine-producing microglia have an altered beta-amyloid load in aged APP/PS1 Tg mice. Brain Behav Immun 2015;48:86–101.
[53] Manocha GD, Floden AM, Rausch K, Kulas JA, McGregor BA, Rojanathammanee L, et al. APP regulates microglial phenotype in a mouse model of Alzheimer's disease. J Neurosci 2016;36:8471–86.
[54] Hong S, Beja-Glasser VF, Nfonoyim BM, Frouin A, Li S, Ramakrishnan S, et al. Complement and microglia mediate early synapse loss in Alzheimer mouse models. Science 2016;352:712–6.
[55] Volianskis A, Kostner R, Molgaard M, Hass S, Jensen MS. Episodic memory deficits are not related to altered glutamatergic synaptic transmission and plasticity in the CA1 hippocampus of the APPswe/PS1deltaE9-deleted transgenic mice model of ss-amyloidosis. Neurobiol Aging 2010;31:1173–87.
[56] Jackson RJ, Rudinskiy N, Herrmann AG, Croft S, Kim JM, Petrova V, et al. Human tau increases amyloid beta plaque size but not amyloid beta-mediated synapse loss in a novel mouse model of Alzheimer's disease. Eur J Neurosci 2016;44:3056–66.
[57] Webster SJ, Bachstetter AD, Nelson PT, Schmitt FA, Van Eldik LJ. Using mice to model Alzheimer's dementia: an overview of the clinical disease and the preclinical behavioral changes in 10 mouse models. Front Genet 2014;5:88.
[58] Francis F, Koulakoff A, Boucher D, Chafey P, Schaar B, Vinet MC, et al. Doublecortin is a developmentally regulated, microtubule-associated protein expressed in migrating and differentiating neurons. Neuron 1999;23:247–56.
[59] Gleeson JG, Lin PT, Flanagan LA, Walsh CA. Doublecortin is a microtubule-associated protein and is expressed widely by migrating neurons. Neuron 1999;23:257–71.
[60] Rubio A, Belles M, Belenguer G, Vidueira S, Farinas I, Nacher J. Characterization and isolation of immature neurons of the adult mouse piriform cortex. Dev Neurobiol 2016;76:748–63.
[61] Klempin F, Kronenberg G, Cheung G, Kettenmann H, Kempermann G. Properties of doublecortin-(DCX)-expressing cells in the piriform cortex compared to the neurogenic dentate gyrus of adult mice. PLoS One 2011;6:e25760.
[62] Bloch J, Kaeser M, Sadeghi Y, Rouiller EM, Redmond DE Jr, Brunet JF. Doublecortin-positive cells in the adult primate cerebral cortex and possible role in brain plasticity and development. J Comp Neurol 2011;519:775–89.
[63] Kremer T, Jagasia R, Herrmann A, Matile H, Borroni E, Francis F, et al. Analysis of adult neurogenesis: evidence for a prominent "non-neurogenic" DCX-protein pool in rodent brain. PLoS One 2013;8:e59269.
[64] Nakagomi T, Molnar Z, Taguchi A, Nakano-Doi A, Lu S, Kasahara Y, et al. Leptomeningeal-derived doublecortin-expressing cells in post-stroke brain. Stem Cells Dev 2012;21:2350–4.
[65] Arvidsson A, Collin T, Kirik D, Kokaia Z, Lindvall O. Neuronal replacement from endogenous precursors in the adult brain after stroke. Nat Med 2002;8:963–70.
[66] Kunze A, Achilles A, Keiner S, Witte OW, Redecker C. Two distinct populations of doublecortin-positive cells in the perilesional zone of cortical infarcts. BMC Neurosci 2015;16:20.
[67] Boulanger JJ, Messier C. Doublecortin in oligodendrocyte precursor cells in the adult mouse brain. Front Neurosci 2017;11:143.
[68] Vukovic J, Borlikova GG, Ruitenberg MJ, Robinson GJ, Sullivan RK, Walker TL, et al. Immature doublecortin-positive hippocampal neurons are important for learning but not for remembering. J Neurosci 2013;33:6603–13.
[69] Bennett ML, Bennett FC, Liddelow SA, Ajami B, Zamanian JL, Fernhoff NB, et al. New tools for studying microglia in the mouse and human CNS. Proc Natl Acad Sci U S A 2016;113:E1738–E1746.
[70] Parakalan R, Jiang B, Nimmi B, Janani M, Jayapal M, Lu J, et al. Transcriptome analysis of amoeboid and ramified microglia isolated from the corpus callosum of rat brain. BMC Neurosci 2012;13:64.
[71] des Portes V, Pinard JM, Billuart P, Vinet MC, Koulakoff A, Carrie A, et al. A novel CNS gene required for neuronal migration and involved in X-linked subcortical laminar heterotopia and lissencephaly syndrome. Cell 1998;92:51–61.
[72] Gleeson JG, Allen KM, Fox JW, Lamperti ED, Berkovic S, Scheffer I, et al. Doublecortin, a brain-specific gene mutated in human X-linked lissencephaly and double cortex syndrome, encodes a putative signaling protein. Cell 1998;92:63–72.
[73] Colonna M, Wang Y. TREM2 variants: new keys to decipher Alzheimer disease pathogenesis. Nat Rev Neurosci 2016;17:201–7.
[74] Hart AD, Wyttenbach A, Perry VH, Teeling JL. Age related changes in microglial phenotype vary between CNS regions: grey versus white matter differences. Brain Behav Immun 2012;26:754–65.
[75] Villeda SA, Luo J, Mosher KI, Zou B, Britschgi M, Bieri G, et al. The ageing systemic milieu negatively regulates neurogenesis and cognitive function. Nature 2011;477:90–4.
[76] Billadeau DD, Nolz JC, Gomez TS. Regulation of T-cell activation by the cytoskeleton. Nat Rev Immunol 2007;7:131–43.
[77] Burkhardt JK, Carrizosa E, Shaffer MH. The actin cytoskeleton in T cell activation. Annu Rev Immunol 2008;26:233–59.
[78] Neumann H, Medana IM, Bauer J, Lassmann H. Cytotoxic T lymphocytes in autoimmune and degenerative CNS diseases. Trends Neurosci 2002;25:313–9.
[79] Rogers J, Luber-Narod J, Styren SD, Civin WH. Expression of immune system-associated antigens by cells of the human central nervous system: relationship to the pathology of Alzheimer's disease. Neurobiol Aging 1988;9:339–49.
[80] Dansokho C, Ait Ahmed D, Aid S, Toly-Ndour C, Chaigneau T, Calle V, et al. Regulatory T cells delay disease progression in Alzheimer-like pathology. Brain 2016;139:1237–51.
[81] Marsh SE, Abud EM, Lakatos A, Karimzadeh A, Yeung ST, Davtyan H, et al. The adaptive immune system restrains Alzheimer's disease pathogenesis by modulating microglial function. Proc Natl Acad Sci U S A 2016;113:E1316–25.